Loss of acoustic black hole effect in a structure of finite size

Cite as: Appl. Phys. Lett. **109**, 014102 (2016); https://doi.org/10.1063/1.4955127
Submitted: 03 May 2016 . Accepted: 20 June 2016 . Published Online: 05 July 2016

Liling Tang, and Li Cheng

Loss of acoustic black hole effect in a structure of finite size

Liling Tang and Li Cheng[a)]
Department of Mechanical Engineering, The Hong Kong Polytechnic University, Hung Hom, Kowloon, Hong Kong

(Received 3 May 2016; accepted 20 June 2016; published online 5 July 2016)

The Acoustic Black Hole (ABH) effect takes place in thin-walled structures with diminishing thickness as a result of the reduction in the bending wave speed. It was shown to exist as a broadband phenomenon, based on wave propagation theory in structures of semi-infinite size. The ABH effect exhibits appealing features for various applications, such as passive vibration control, energy harvesting, and sound radiation control. In this paper, we demonstrate the disappearance of the ABH effect in a finite beam at specific frequency ranges above the cut-on frequency, both experimentally and theoretically. Analyses show that the phenomenon takes place at frequencies which are close to the low order local resonant frequencies of the portion of the beam demarcated by the position of the excitation force. These frequencies can be predicted so that the phenomenon can be avoided for the targeted frequency ranges in ABH applications. *Published by AIP Publishing.*
[http://dx.doi.org/10.1063/1.4955127]

The Acoustic Black Holes (ABH) effect, the acoustic analogy of astrophysical black holes,[1–3] takes place through a gradual reduction in the phase velocity of the bending wave as a result of thickness thinning in a structure. In the ideal scenario where the structural thickness is tailored according to the power law $h(x) = \varepsilon x^m$ with $m \geq 2$, wave speed approaches zero at the wedge tip, thus warranting quasi zero wave reflection.[4,5] The similar concept is also used in optics to achieve the optic black hole.[6] The resulting high energy concentration is conducive to various applications, such as passive vibration control,[7–15] energy harvesting,[16,17] and sound radiation control.[18,19] In addition, ABHs can be embedded into phononic thin plates to achieve remarkable dispersion properties.[20]

An ideal ABH structure cannot be achieved because of the manufacturing limitations, thus resulting in an unavoidable truncation at the wedge tip. The existence of the truncation would greatly weaken the ABH effect by generating wave reflection.[5,7] This, however, can be compensated for with the help of thin damping layers to some extent.[8,10–14] Existing research indicates that, despite the truncation, the ABH effect is still highly efficient as a broadband phenomenon, although the effect is not obvious below the cut-on frequency.[21] For semi-infinite structures with ABH wedge features, the geometrical acoustic approach[22] was first proposed to analyze the flexural wave propagation properties and revealed an obvious reduction in the reflection coefficient with the increase of frequency.[5,7] Similar results on the reflection coefficient were also obtained by an impedance method[9] without the limitation of the hypothesis of geometrical acoustics.[23] However, these two types of approaches only deal with semi-infinite structures, namely, the finite length in the wedge and the infinite length on the other portion of the structure. In practice, structures are always finite in size with real structural boundaries. In such cases, multiple reflections would take place between the boundaries and excitation points as well as the intersection between the ABH portion and the rest of the structure. Up to now, the reported theoretical models[8,24] and experiments[10–15] on finite structures with ABH profiles all confirmed the effectiveness of the ABH effect above the cut-on frequency. In this paper, however, we experimentally demonstrate that the ABH effect may lose its effect, or fail, in a finite beam in particular frequency bands, which will be called failure frequency bands hereafter. A previously developed wavelet-decomposed energy mothed[25] is used to confirm and explain this phenomenon and to predict the failure frequency bands, which should be avoided in applications.

A beam with a tailored ABH profile wedge was employed to investigate its flexural vibration response when subjected to a unit point excitation force. Fig. 1 shows the experimental setup. According to the coordinate system defined in Fig. 1, the beam consists of a left ABH part with a symmetrical thickness profile $h(x) = 0.00125x^2$, 12 cm long, and a right uniform part with a constant thickness of 0.64 cm, 16 cm long. The whole beam has a uniform width of 1 cm and is made of steel with a mass density of 7794 kg/m^3 and Young modulus of 200 GPa. The beam was hung by two thin strings, as illustrated in Fig. 1, to mimic free boundary conditions. An electromagnetic shaker was placed at 8 cm away

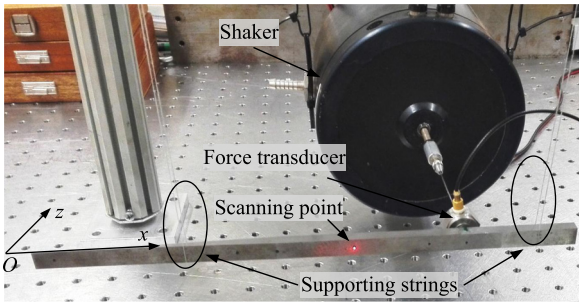

FIG. 1. Experimental setup. A beam with a left ABH part and a right uniform part was hung by two thin strings and excited by a periodic chirp signal from an electromagnetic shaker at the point, 8 cm away from the uniform end; the force was measured by a force transducer and amplified by a charge amplifier; a Polytec scanning laser vibrometer was used to scan the beam and measure its vibration response.

[a)]Author to whom correspondence should be addressed. Electronic mail: li.cheng@polyu.edu.hk.

from the uniform end of the beam, with the excitation force measured by a force transducer (B&K 8200) and amplified by a charge amplifier (B&K 2635). A periodic chirp signal with frequency from 0 Hz to 16 kHz was used to feed the shaker via a power amplifier (B&K 2706). A Polytec scanning laser vibrometer was used to scan the whole beam for the response measurement.

Experimental results in Fig. 2(a) reveal that the mean quadratic velocity of the ABH part, representing its overall vibration level, is particularly low in two regions around 3595 Hz and 11 290 Hz, respectively. In Fig. 2(b), the ratio of the mean quadratic velocity of the ABH part to that of the uniform beam part, defined as $\Gamma = 10\log\frac{\langle V^2\rangle_{\mathrm{ABH}}}{\langle V^2\rangle_{\mathrm{Unif}}}$, is used to quantify the effectiveness of the ABH effect, on the premise that effective ABH effect results in energy concentration in the tapered ABH region with a high positive Γ. On the contrary, when Γ is negative, we consider the ABH effect is lost or sufficiently weak, in which case we loosely call it failure of the ABH effect. As clearly seen in the Fig. 2(b), around these two bottommost frequency regions the energy mainly concentrates on the uniform part rather than the ABH part as the conventional ABH effect would have suggested. This indicates a clear disappearance of effectiveness of the ABH effect around these frequencies, against the conventionally established broadband nature of the ABH feature reported in the literature.[8,10–15,24] A band is defined as a failure band when its Γ value is negative. In the present case, the two failure bands are 875 Hz and 1755 Hz, respectively.

To confirm and understand the aforementioned observation, numerical simulations are performed using our previously developed wavelet-decomposed and energy-based model.[25] Based on the Euler–Bernoulli beam theory, the displacement field of the beam is expressed as $\{u, w\} = \left\{-z\frac{\partial w}{\partial x}, w(x,t)\right\}$, where the flexural displacement w is expanded over the Mexican hat wavelet (MHW) functions $\varphi_{j,k}(x)$ as[26]

$$w(x,t) = \sum_{j=0}^{m}\sum_{k} a_{j,k}(t)\varphi_{j,k}(x), \tag{1}$$

with $\varphi_{j,k}(x) = \frac{2}{\sqrt{3}}\pi^{-\frac{1}{4}}2^{j/2}\left[1-(2^j x-k)^2\right]\mathrm{e}^{-\frac{(2^j x-k)^2}{2}}$.

The kinetic energy E_k, the potential energy E_p, and the work done by the applied force W can be mathematically expressed as a function w to form the Lagrangian of the system $L = E_k - E_p + W$. Substituting L into the Lagrange's equations $\frac{\mathrm{d}}{\mathrm{d}t}\left(\frac{\partial L}{\partial \dot{a}_{j,k}(t)}\right) - \frac{\partial L}{\partial a_{j,k}(t)} = 0$ and simplifying the equations in the harmonic regime, we can get the vibration response by solving the following matrix equation:

$$[\mathbf{K} - \omega^2\mathbf{M}]\mathbf{A} = \mathbf{F}, \tag{2}$$

where $\mathbf{K}$ and $\mathbf{M}$ are, respectively, the stiffness matrix and mass matrix, $\mathbf{A}$ and $\mathbf{F}$ are, respectively, the vectors of the response and the force.

The simulated results under the same experimental condition are shown in Fig. 2 to compare with the experimental ones. Both sets of results agree well, especially below 8000 Hz. Most importantly, the simulated results confirm the existence of the two ABH failure bands. Note that the numerically predicted second frequency band is more obvious than that from the experiment. The discrepancies between them are likely due to the neglected shear and torsional effect in the simulation, which certainly exists and comes into play at high frequencies. It was observed that the inevitable deviation of the excitation point from the enteral axis of the beam also enhances the problem, by introducing slight torsional deformation of the beam, which is not considered in the model. Nevertheless, the existence of the ABH failure bands is unequivocally demonstrated.

To further demonstrate the phenomenon, Figs. 3(a) and 3(b) depict the experimental and simulated displacement distribution of the beam at the first and second bottommost frequencies, for two excitation locations ($x_f = 24$ cm and 26 cm, respectively). As a comparison, Fig. 3(c) also depicts the displacement distribution at two frequencies, outside and adjacent to the two failure bands, respectively ($f = 3220$ Hz and 5840 Hz). Fig. 3(c) shows typical ABH effect in that the vibration mainly concentrates on the ABH part with large vibration level near the wedge tip. However, the highly consistent results in Figs. 3(a) and 3(b) show that the vibration level of the ABH part at two bottommost frequencies is negligible compared with that of the uniform part, which indicates a loss of the ABH effect. It is logical to surmise that, in this situation, applying damping layers or energy harvesting elements on the ABH part would not lead to efficient damping or harvesting performance. For both excitation positions, the figure shows that the low vibration region of the ABH part roughly starts from the excitation location.

A plausible reason to explain the observed phenomenon is proposed as follows. Due to the presence of the excitation, a structural discontinuity in the local impedance is created,

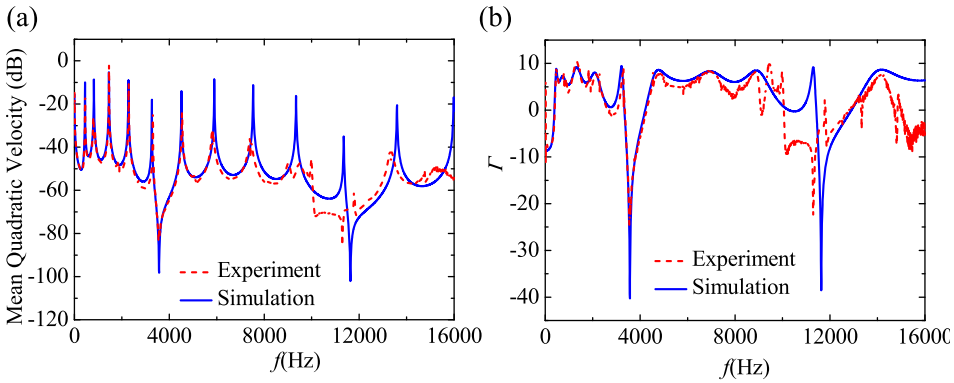

FIG. 2. (a) The mean quadratic velocity of the ABH part and (b) the ratio of mean quadratic velocity of the ABH part to that of the uniform beam part from experimental and numerical simulations.

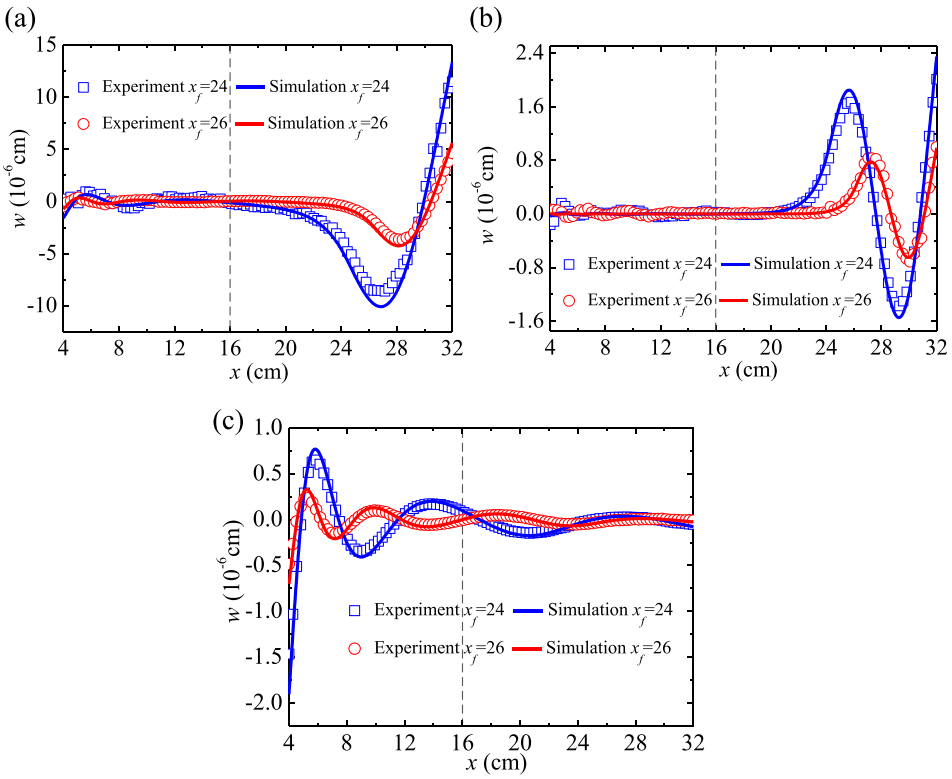

FIG. 3. The experimentally measured and numerically predicted displacement distribution along the beam at (a) the first bottommost frequency and (b) the second bottommost frequency of the energy ratio Γ where the ABH effect fails, and (c) the frequencies outside and adjacent to the first failure bands ($f = 3220$ Hz and 5840 Hz), with the force applied at $x_f = 24$ cm and $x_f = 26$ cm, respectively. Left to the gray dashed line is the ABH part and the right is the uniform part.

demarcating the beam into two subsystems, i.e., the right uniform part and the left part with ABH profile. Within the failure frequency band, multiple wave reflections take place between the structure boundary and the excitation point. This allows the formation of standing waves and local resonances, thus triggering the energy localization effect. Indeed, analyses show that the ABH failure frequencies correspond to the local resonance frequencies of that uniform beam portion with pinned boundary conditions at the force excitation point and the real structural boundary at the other end. In the present case, the observed two bottommost ABH failure frequencies correspond to the first two local resonance frequencies of the beam portion with the pinned-free boundary, which can be predicted.[27] When the excitation frequency approaches the local resonance frequencies of the uniform portion delimited by the excitation point and the structural boundary, energy will be localized within that region due to the local resonance phenomenon, neutralizing the ABH effect in the ABH beam portion. To further confirm this phenomenon and explanation, we changed the excitation point to $x_f = 26$ cm (6 cm away from the end of the uniform beam portion). In this case, the first and second local resonant frequencies of the uniform beam portion are re-calculated, giving 6380 Hz and 20 673 Hz, respectively. These values are reasonably close to the two bottommost frequencies corresponding to the minimum energy ratio Γ (6422 Hz and 19 844 Hz). The predicted and experimentally measured displacement distributions are also in excellent agreement, as shown in Fig. 3.

More cases were simulated to confirm the general character of the phenomenon and the validity of the proposed prediction of the failure frequencies. When changing the boundary conditions and excitation locations, similar ABH failure phenomenon was noticed in each case (not shown here). The first and second bottommost ABH failure frequencies are compared with the corresponding predicted local resonant frequencies of the uniform subsystem delimited by the excitation points at $x_f = 23$ cm and $x_f = 27$ cm, respectively, as displayed in Table I. Treating the excitation point as a pinned constraint, the predicted local resonant frequencies are indeed very close to bottommost ABH failure frequencies for all three different boundary conditions. The failure frequency bands are also highly obvious, ranging from 542 Hz to as large as 2594 Hz. Therefore, the reported ABH failure phenomenon applies to all cases and the phenomenon can be accurately reproduced by the established wavelet-decomposed model.

In summary, we observed, both experimentally and numerically, the loss of the ABH effect in a beam of finite size, which up to now has been reported as a broadband phenomenon above the cut-on frequency in semi-infinite ABH structures. The loss of the ABH effect, also referred to as ABH failure in this paper, features a significantly impaired energy focalization capability in the tapered ABH region. The width of the failure band can be quite substantial. When this happens, the vibration energy mainly concentrates within the uniform part of the beam delimited by the excitation force, thus neutralizing the expected ABH effect. Physically, the presence of the shaker, or mechanical excitation, introduces a discontinuity in the local structural impedance to the waves. At certain frequencies (within the failure frequency bands), multiple wave reflections take place between the structure boundary and the excitation point, forming standing waves and local resonances, thus triggering the localization effect. The previously developed wavelet-decomposed and energy-based model confirmed the general character of the phenomenon. The failure frequencies can be predicted by calculating the local resonance frequencies of the beam

TABLE I. The first and second bottommost ABH failure frequencies and their comparison with corresponding predicted local resonant frequencies of the uniform beam portion delimited by the excitation points $x_f = 23$ cm and $x_f = 27$ cm, respectively, and failure frequency bands for three different boundary conditions.

Boundary conditions	Equivalent local boundary conditions	Excitation locations (cm)	Predicted local resonant frequencies (Hz)	Bottommost ABH failure frequencies (Hz)	Difference (%)	Failure frequency bands (Hz)
Free-free	Pinned-free	$x_f = 23$	2835	2821	0.50	717
			9188	9188	0	1202
		$x_f = 27$	9186	9122	0.70	1296
			29 769	29 774	−0.00017	2594
Free-pinned	Pinned-pinned	$x_f = 23$	1815	1821	−0.33	542
			7260	7260	0	1999
		$x_f = 27$	5880	5880	0	1205
			23 521	23 520	0.0043	2170
Free-clamped	Pinned-clamped	$x_f = 23$	2835	2858	−0.81	721
			9188	9176	0.13	1206
		$x_f = 27$	9186	9136	0.54	1390
			29 769	29 712	0.00019	2016

portion delimited and pinned by the excitation point, which allows the avoidance of the phenomenon in the targeted application ranges.

The work was supported by the Research Grant Council of the Hong Kong SAR (PolyU 152009/15E), National Natural Science Foundation of China (No. 11532006), and the NUAA State Key Laboratory Program under Grant Nos. MCMS-0514K01 and MCMS-0516K02. The authors thank Jassy Cheng for his help in polishing the paper.

[1]B. Horstman, B. Reznik, S. Fagnocchi, and J. I. Cirac, Phys. Rev. Lett. **104**, 250403 (2010).
[2]I. Carusotto, S. Fagnocchi, A. Recati, R. Balbinot, and A. Fabbri, New J. Phys. **10**, 103001 (2008).
[3]O. Lahav, A. Itah, A. Blumkin, C. Gordon, S. Rinott, A. Zayats, and J. Steinhauer, Phys. Rev. Lett. **105**, 240401 (2010).
[4]M. A. Mironov, Sov. Phys. - Acoust. **34**, 318 (1988).
[5]V. V. Krylov and F. J. B. S. Tilman, J. Sound Vib. **274**, 605 (2004).
[6]E. E. Narimanov and A. V. Kildishev, Appl. Phys. Lett. **95**, 041106 (2009).
[7]V. V. Krylov, Acta Acust. United Acust. **90**, 830 (2004).
[8]D. J. O'Boy and V. V. Krylov, J. Sound Vib. **330**, 2220 (2011).
[9]V. B. Georgiev, J. Cuenca, F. Gautier, L. Simon, and V. V. Krylov, J. Sound Vib. **330**, 2497 (2011).
[10]V. V. Krylov and R. E. T. B. Winward, J. Sound Vib. **300**, 43 (2007).
[11]D. J. O'Boy, E. P. Bowyer, and V. V. Krylov, J. Acoust. Soc. Am. **129**, 3475 (2011).
[12]E. P. Bowyer, D. J. O'Boy, V. V. Krylov, and J. L. Horner, Appl. Acoust. **73**, 514 (2012).
[13]V. Denis, A. Pelat, and F. Gautier, J. Sound Vib. **362**, 56 (2016).
[14]J. J. Bayod, J. Vib. Acoust. **133**, 061003 (2011).
[15]E. P. Bowyer and V. V. Krylov, Compos. Struct. **107**, 406 (2014).
[16]L. X. Zhao, S. C. Conlon, and F. Semperlotti, Smart Mater. Struct. **23**, 065021 (2014).
[17]L. X. Zhao, S. C. Conlon, and F. Semperlotti, Smart Mater. Struct. **24**, 065039 (2015).
[18]E. P. Bowyer and V. V. Krylov, Appl. Acoust. **88**, 30 (2015).
[19]S. C. Conlon and J. B. Fahnline, J. Acoust. Soc. Am. **137**, 447 (2015).
[20]H. F. Zhu and F. Semperlotti, Phys. Rev. B **91**, 104304 (2015).
[21]O. Aklouche, A. Pelat, S. Maugeais, and F. Gautier, J. Sound Vib. **375**, 38 (2016).
[22]V. V. Krylov, Sov. Phys. - Tech. Phys. **35**, 137 (1990).
[23]P. A. Feurtado and S. C. Conlon, J. Acoust. Soc. Am. **136**, EL148 (2014).
[24]D. J. O'Boy and V. V. Krylov, Appl. Acoust. **104**, 24 (2016).
[25]L. L. Tang, L. Cheng, H. L. Ji, and J. H. Qiu, J. Sound Vib. **374**, 172 (2016).
[26]T. Hou and H. Qin, Graphical Models **74**, 221 (2012).
[27]S. S. Rao and F. F. Yap, *Mechanical Vibrations* (Addison Wesley, Massachusetts, 1995), pp. 439–444.